9.1. Introduction

The present Chapter discusses the effect of Ni and Cr on the performance of pristine Zinc cobaltite matrix. Nickel is chosen as another dopant due to the fact that it is also a transition element and it has performed well in Zinc cobaltite which is also a spinel structure **(Ahsan et al., 2020)**. Double dopants is chosen to increase the stability of the structure and to create vacancies to improve the electrochemical performance.

9.2. X-Ray Diffraction Analysis of Ni,Cr:$ZnCo_2O_4$

The structural impact of Zinc cobaltite due to the addition of Ni and Cr dopants have been characterized by XRD analysis. The Rietveld refinement has been carried out to evaluate the structural changes on doping. In this case, doping of Zinc cobaltite with Ni and Cr elements have been prepared by sol-gel method achieving a single phase, Figure 68. Similar features have been obtained for pure $ZnCo_2O_4$ and Fe and Cr doped $ZnCo_2O_4$ described in previous Chapters (7 and 8) of this research work. The presence of single phase after Ni and Cr doping has been verified by the good fit of Rietveld refinement (W_R=3.133 and GOF=1.00) and the parameters are tabulated in Table 28. The generated (hkl) values from the Rietveld analysis have been indexed by the corresponding diffraction planes of the Ni and Cr doped $ZnCo_2O_4$. The spinel cubic crystal structure of Ni and Cr doped sample remains unchanged as observed in pure and Fe and Cr doped material.

However, the positional coordinates of Zn have been altered for the Ni and Cr doped $ZnCo_2O_4$ sample. For Ni, Cr: $ZnCo_2O_4$ sample, the positional coordinates of Zn are (0.1250, 0.1250, 0.1250), Ni are (0.0181, 0.0181, 0.0181), Cr are (0.0110, 0.0110, 0.0110), Co are (0.6250, 0.6250, 0.6250) and O are (0.3652, 0.3652, 0.3652) respectively. The Zn, Co and O positions are not changed compared to the Fe, Cr doped $ZnCo_2O_4$. Figure 69 shows the corresponding crystal structure generated from VESTA software. The inset of Figure 69 illustrates the structure of a doped sample without cobalt atoms so that the location of the oxygen atom can be visualised.

Parameters calculated from XRD analysis are given in Table 29. The crystallite size can be determined by the Debye-Scherrer formula using FWHM of (311) plane. From Table 23, it is clear that the β value of Ni, Cr: $ZnCo_2O_4$ sample is 0.35°. It is higher than the pure $ZnCo_2O_4$ and Fe and Cr doped $ZnCo_2O_4$ which affects the crystallite size of the sample. Highest β value decreases the crystallite size of Ni and Cr doped $ZnCo_2O_4$ sample.

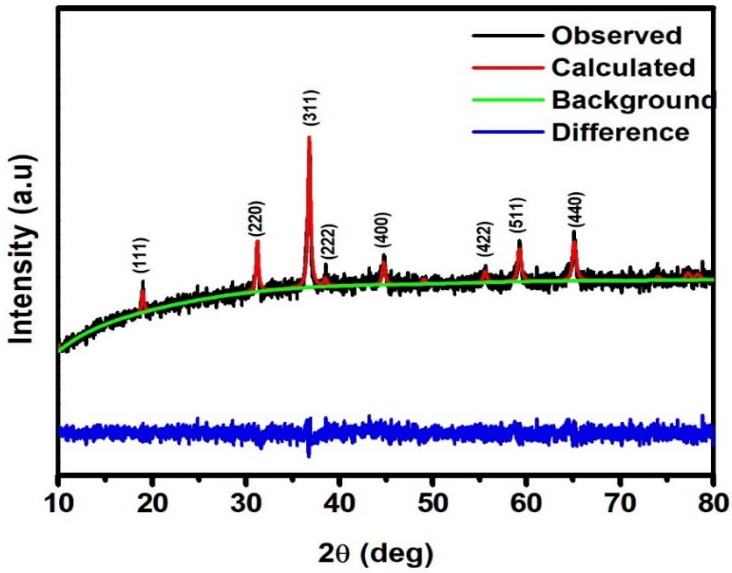

Figure 68 - Rietveld refined X-ray Diffractogram of Ni,Cr:$ZnCo_2O_4$

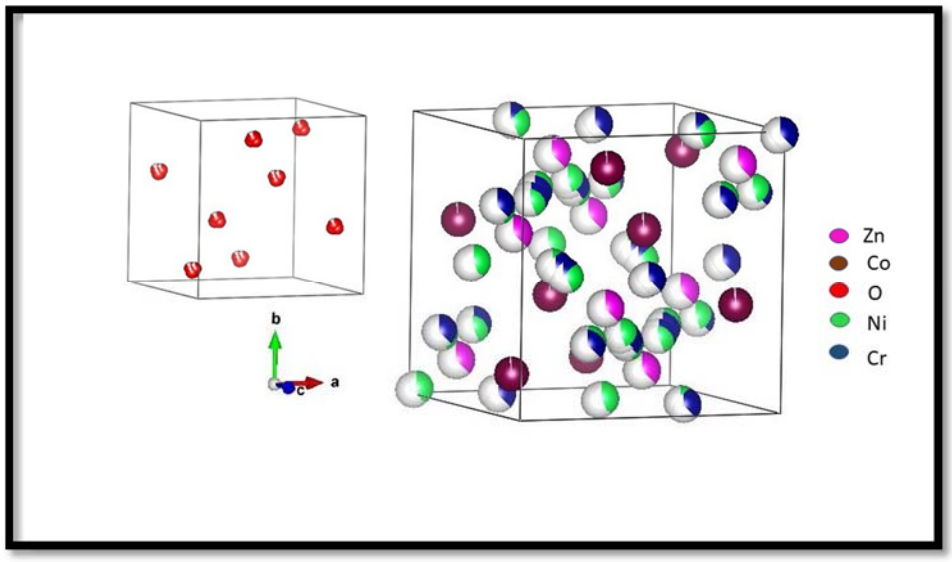

Figure 69 - Rietveld refined crystal structure of Ni,Cr:$ZnCo_2O_4$; inset shows the position of oxygen

Table 28 - Parameters obtained from the Rietveld refinements for Ni,Cr: $ZnCo_2O_4$

Sample/Parameter	**Ni, Cr: $ZnCo_2O_4$**
Crystal system /Space group	$Fd\bar{3}m$
Cell parameter (Å)	a=b=c=8.0985
Cell Volume ($Å^3$)	531.163
Co-Ordinates (x, y, z)	Zn (0.125, 0.125, 0.125) Co (0.625, 0.625, 0.625) O (0.3652, 0.3652, 0.3652) Ni (0.0181, 0.0181, 0.0181) Cr (0.0110,0.0110,0.0110)
Occupancy	Zn 0.303;Ni 0.430;Cr 0.379; Co 0.973; O 0.875
Density (gm cm^{-3})	7.958
α, β, γ	90°
W_R	3.133
GOF	1.00

Table 29 - Parameters calculated from the X-ray diffractogram of Ni,Cr:$ZnCo_2O_4$

Sample / Parameter	**2θ (311) (°)**	**β (311) (°)**	**d (311) (Å)**	**Crystallite size (nm)**	**Strain (ε)**	**Dislocation density ($x10^{15}$)/cm^3**
Ni,Cr: $ZnCo_2O_4$	36.85	0.35	2.43	22.46	0.27	1.98

The calculated crystallite size of Ni and Cr doped $ZnCo_2O_4$ from Debye Scherrer formula is in the range of 22 nm. In addition to changes observed in β value, the lattice parameter value 'a' of the Ni, Cr: $ZnCo_2O_4$ has been altered. It has a value of 8.0985 Å which is almost similar with $ZnCo_2O_4$ (a = 8.0859 Å) and Fe, Cr: $ZnCo_2O_4$ (a = 8.0945 Å). The occupancy of Zn, Ni and Cr shows a bit more than the actual occupancy of pristine indicating that the volume change is accommodated at the cost of Co and O occupancies. Per unit cell the total of Zn, Ni and Cr, 10 atoms are present other than Co and O as in pristine and Fe, Cr doped $ZnCo_2O_4$. Due to the smaller number of atoms per unit cell, more interspace is expected here too. The vacancy created due to Ni and Cr doping is 20% per unit cell. Unlike Fe, Cr doped structure, Ni, Cr has less octahedral occupancy and tetrahedral occupancy which can be very clearly seen from the crystal structure of unit cell drawn with Vesta software using the Rietveld results.

9.3. Raman Analysis of Ni,Cr:$ZnCo_2O_4$

The Raman spectrum of Ni and Cr doped Zinc cobaltite further clarifies the structural aspects, which are shown in Figure 70. The observed Raman bands in the doped system have been shifted when compared to the pure Zinc cobaltite due to environmental change in the occupancy of dopant atoms as discussed in the previous Chapter. The corresponding Raman shifts for the Ni, Cr:$ZnCo_2O_4$ sample are given in Table 30. Apart from the peak shift, the Raman spectrum of the Ni and Cr doped sample does not show any additional peaks. It indicates that the existence of single phase in the Ni, Cr:$ZnCo_2O_4$ sample, which has been evidenced by the XRD analysis. All the peaks have been widened suggesting the stress induced by dopants such as Ni and Cr elements as broadening occurs due to the phonons due to atoms not in zone center. The 610 cm^{-1} peak has merged with the 649cm^{-1} peak to show a broad peak at 649 cm^{-1} indicating that the $F_{2g}(1)$ mode has intensified thus enveloped with the A1g mode of oscillation. The $F_{2g}(1)$ is intense due to the occupation of octahedral sites by the dopant Ni in this case which does not bind the Co of tetrahedral site allowing the oxygen to oscillate in this mode. Whereas, occupancy of Fe at this octahedral site might have bound to the Co preventing the freedom of F_{2g} mode of oscillation in the Fe,Cr doped $ZnCo_2O_4$ case.

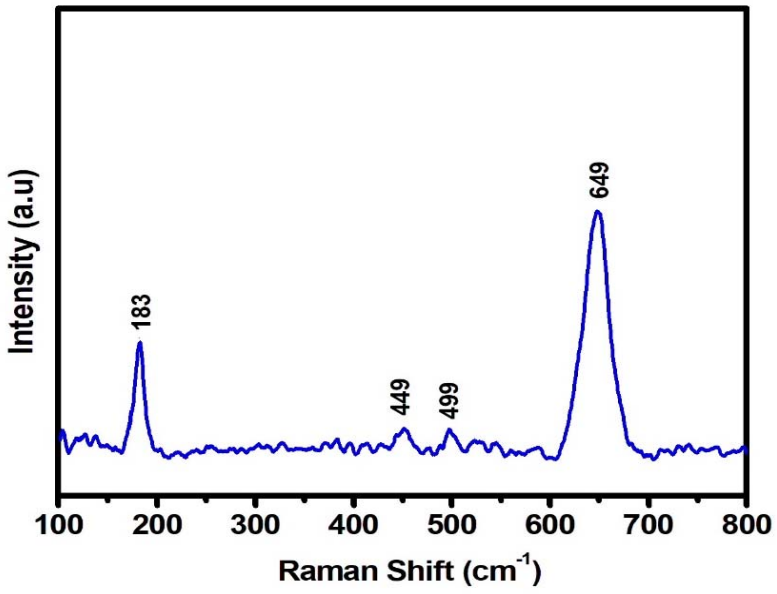

Figure 70 - Raman spectra of Ni,Cr:$ZnCo_2O_4$

Table 30 - Assignments of Raman peaks of Ni,Cr:$ZnCo_2O_4$

Raman Band (cm^{-1})	Symmetry species	Assignment
183	F_{2g} (3)	δ(Zn-O)
449	E_g	ν (Co-O) + ν (Zn-O)
599	F_{2g} (2)	ν(Co-O)
610	F_{2g}(1)	V(Co-O) Not well resolved
649	A_{1g}	ν(Co-O)

9.4. FESEM Analysis of Ni,Cr:$ZnCo_2O_4$

The effect of dopants on the morphological analysis of Ni and Cr doped Zinc cobaltite is shown in Figure 71. The octahedral shaped grains are seen in micrographs of Ni and Cr doped sample. The grains are heterogeneously distributed on the surface of the sample. However, compared to bare Zinc cobaltite and Fe and Cr doped Zinc cobaltite, there are a greater number of smaller grains distributed which is well seen in FESEM micrograph at x 35000 magnification of 1µm scale. From FESEM analysis, it is clear that doping the pure Zinc cobaltite with Ni and Cr significantly diversifies the size of grains and shows more number of smaller grains across the sample, as seen in Figure 71. This decrease in crystallite size corroborates with the XRD results.

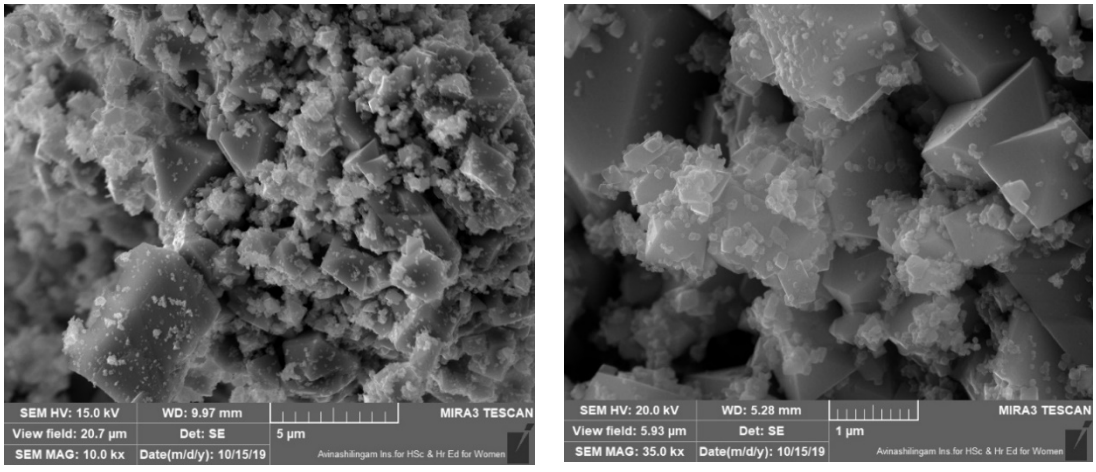

Figure 71 - FESEM micrographs of Ni,Cr:$ZnCo_2O_4$

9.5. Elemental Analysis of Ni,Cr:$ZnCo_2O_4$

Elemental analysis of Ni and Cr doped Zinc cobaltite is shown in Figure 72. It confirms the presence of Zn, Co, O, Ni and Cr in the prepared sample. There are no additional peaks rather than the above-mentioned elements verifying the purity of the sample. It agrees well with XRD and Raman results of spinel structured Ni and Cr doped Zinc cobaltite. The atomic weight of Zn is 1.56% in Ni,Cr doped $ZnCo_2O_4$ which is in good agreement with the number of Zn sites per unit cell of 2.5 which is the share of eight dedicated atoms with the dopant in a unit cell. The atomic weight percent of Fe,Cr doped $ZnCo_2O_4$ is 3.59% which corresponds to 5 atoms of Zn.

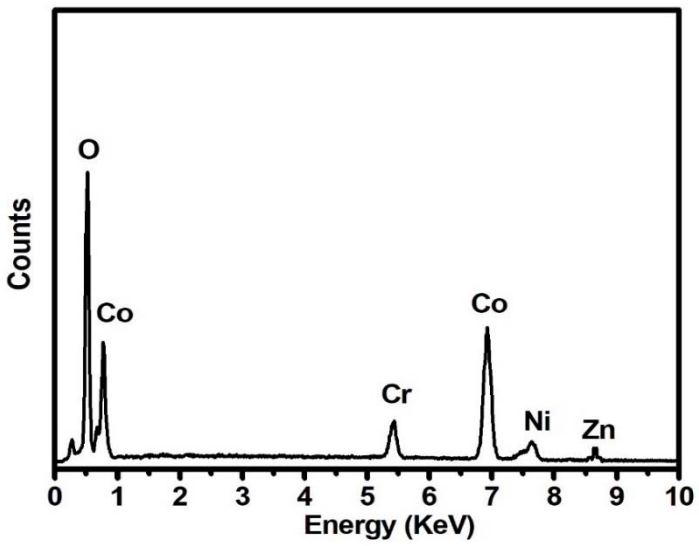

Figure 72 - EDX spectrum of Ni,Cr:$ZnCo_2O_4$

Table 31 - Elemental composition of Ni,Cr:$ZnCo_2O_4$

Elements	Atomic Weight percentage
Zn	1.56
Co	51.64
O	31.92
Ni	3.45
Cr	7.82

Apart from the characteristic lines of Zn, Co and O discussed earlier, the EDX analysis exhibits peaks at 7.477 KeV (Kα line of Ni) and 5.414 KeV (Kα line of Cr) corresponds to the Ni and Cr elements confirms the successful incorporation of the dopants into the host matrix. The atomic weight percentages of the elements present in Ni and Cr doped zinc cobaltite are given in Table 31.

9.6. Electrochemical properties of Ni,Cr:$ZnCo_2O_4$

9.6.1. Cyclic Voltammetry Analysis of Ni,Cr:$ZnCo_2O_4$

The cyclic voltammogram of the Ni,Cr:$ZnCo_2O_4$ sample is performed with aqueous electrolyte, 1M KOH. The coated Ni,Cr:$ZnCo_2O_4$ on Cu foil current collector has been cut into 1×1 cm^2 dimensions utilized as a working electrode. The potential window of the Ni and Cr doped Zinc cobaltite is fixed from 0 V-0.6 V. The corresponding CV graph is given in Figure 73. It is not strictly a rectangular concluding that it exhibits pseudocapacitive behaviour. The potential window of Ni and Cr doped zinc cobaltite is higher than the bare and Fe and Cr doped electrochemical system. Hence, improve the electrochemical performance. The specific capacitance values of Ni and Cr doped Zinc cobaltite are 550, 392, 297, 234, 198 and 190 Fg^{-1} at the scan rate of 10 mV/s, 20 mV/s, 40 mV/ s, 60 mV/s, 80 mV/s and 100 mV/s respectively.

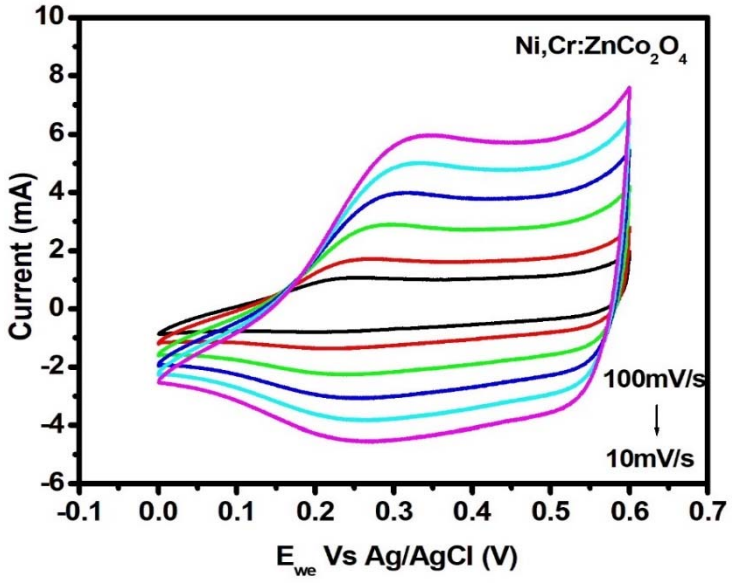

Figure 73 - Cyclic voltammogram of Ni,Cr:$ZnCo_2O_4$

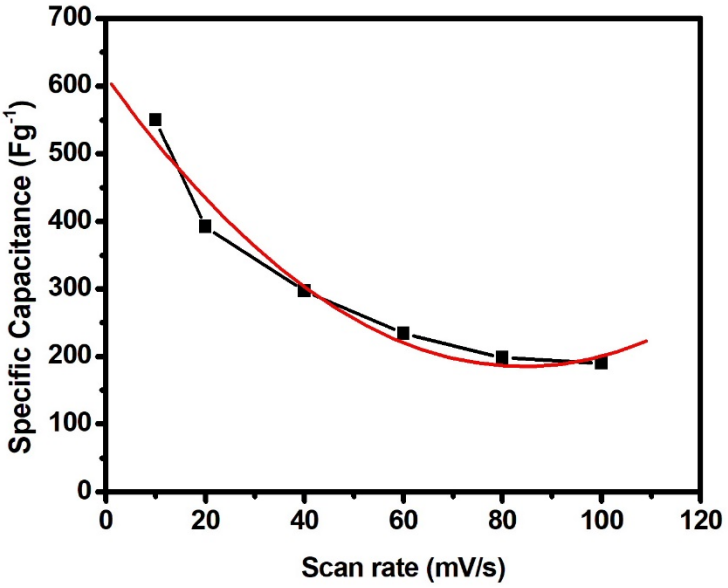

Figure 74 - Plot of scan rate vs specific capacitance of Ni,Cr:$ZnCo_2O_4$

Figure 74 shows the scan rate versus the specific capacitance of the doped sample. As the scan rate increases the specific capacitance decreases, which is similar to that of pure and Fe and Cr doped Zinc cobaltite. This behaviour is due to the rapid redox nature at high scan rates in which there is no sufficient time available for ion transport. The polynomial fit of this scan rate versus specific capacitance results in a quadratic equation ($y= 0.06x^2-10.18x+613.33$) showing dependence of two mechanisms at different scan rates where the real part of the specific capacitance will be 84.12 which indicates better performance of capacitance.

9.6.2. Galvanostatic Charge-Discharge analysis of Ni,Cr:$ZnCo_2O_4$

The charge storage mechanism during the electrochemical process of Ni and Cr doped Zinc cobaltite is confirmed by GCD analysis, Figure 75. The non-linear nature of the GCD curve for Ni and Cr doped zinc cobaltite indicating pseudocapacitive behaviour that goes in hand with the results observed with CV. From the GCD curves, the higher specific capacitance value of 575 Fg^{-1} is reached at a current density of 1 Ag^{-1} for Ni and Cr doped sample. The specific capacitance of the doped sample is compared with the reported $ZnCo_2O_4$, listed in Table 21 (Chapter 6). The results of Chen et al., 2019 (Fg^{-1}), Rajesh et al., 2017 (694 Fg^{-1}) and Fu et al 2015 (689 Fg^{-1}) are comparable to the present work but all the work has been accomplished with Ni foam and hydrothermal/ solvothermal processing.

In contrary, the present work has achieved a commensurate specific capacitance of 575 Fg^{-1} at 1 Ag^{-1} by simple sol-gel method preparation with inexpensive conventional copper collector Moreover, the doped material exhibits nearly twice the specific capacitance value than the pristine material.

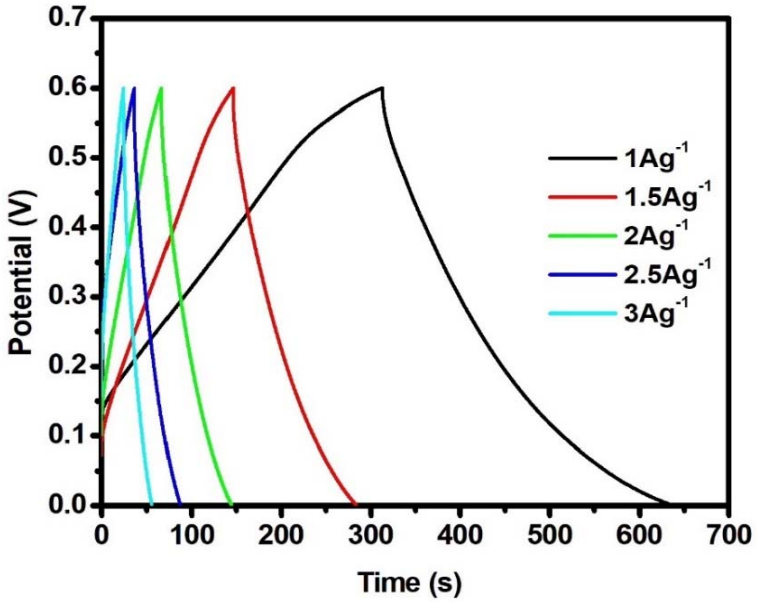

Figure 75 - Galvanostatic Charge-Discharge curves of Ni,Cr:$ZnCo_2O_4$

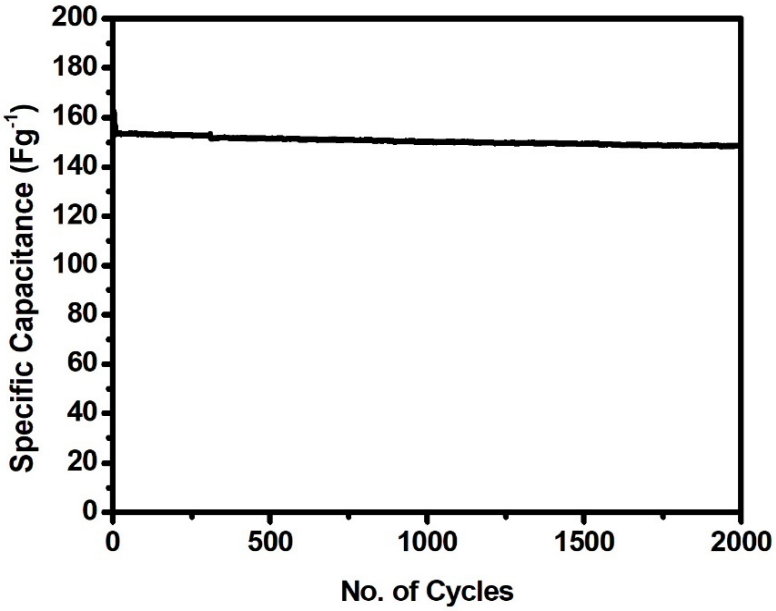

Figure 76 - Cyclic stability of Ni,Cr:$ZnCo_2O_4$

The cyclic stability of Ni, Cr: $ZnCo_2O_4$ has been tested over 2000 cycles and is shown in Figure 76. The Ni and Cr doped $ZnCo_2O_4$ has capacitance retention of 90% at 5 Ag^{-1} for 2000 cycles indicating better electrochemical stability than the pure $ZnCo_2O_4$. When compared to previously reported literature **(Rajesh et al., 2016; Raut & Sankapal, 2017; Xu et al., 2017),** Ni, Cr: $ZnCo_2O_4$ has an excellent cyclic stability than reported ones where pure $ZnCo_2O_4$ has been exploited. Hence the inclusion of Ni and Cr as dopants in $ZnCo_2O_4$ has effectively increased the electrochemical performance of the pure Zinc cobaltite.

9.6.3. Electrochemical Impedance analysis of Ni,Cr:$ZnCo_2O_4$

Electrochemical impedance analysis of Ni and Cr doped $ZnCo_2O_4$ with 1M KOH electrolytic solution is given in Figure 77. As in the previous cases, the semicircle followed by a spike is seen and the impedance plot is fitted with EC- lab software, and the equivalent circuit is same as that of pure zinc cobaltite and Fe,Cr doped $ZnCo_2O_4$.

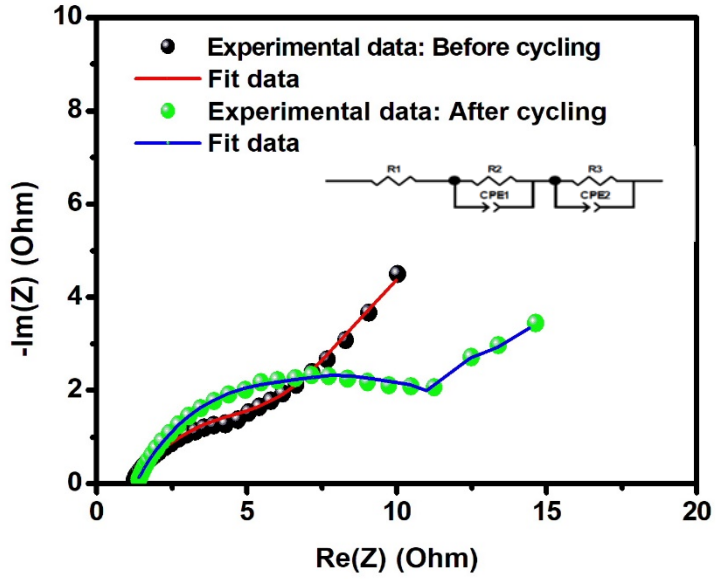

Figure 77 - Electrochemical impedance spectra of Ni,Cr:$ZnCo_2O_4$

Before cycling, the value of solution resistance (R_1) and charge transfer resistance (R_2) for Ni, Cr: $ZnCo_2O_4$ are 1.08 Ω and 1.29 Ω respectively. After cycling, the charge transfer resistance is high which indicates the formation of solid electrode/electrolyte interface. The charge transfer resistance and interfacial resistance (R_3) of the Ni and Cr

doped sample is lower than the pristine and Fe and Cr doped zinc cobaltite. The fitted parameters calculated from the equivalent circuit are given in Table 32. The electrochemical characterizations (CV, GCD and EIS) conclude that the Ni, Cr: $ZnCo_2O_4$ sample exhibits good electrochemical performance when compared with pristine.

Table 32 - Fitted parameters of electrochemical impedance spectra of Ni,Cr:$ZnCo_2O_4$

Parameters	Ni, Cr: $ZnCo_2O_4$	
	Before Cycling	**After Cycling**
$R_1(\Omega)$	1.08	1.29
$R_2(\Omega)$	1.99	10.37
CPE 1	0.23	0.07
n1	0.63	0.73
$R_3(\Omega)$	5.56	67.67
CPE 2	0.02	$9.39 X10^{-3}$
n2	0.47	0.58

The value of CPE1 which corresponds to the interfacial capacitance shows higher value compared to both pure and Fe,Cr doped $ZnCo_2O_4$. The dispersive index n1 well preserves the capacitive behaviour. However, the diffusive element is though lower than the Pristine and Fe,Cr doped $ZnCo_2O_4$ still continues to be diffusive which may be correlated with the Raman result of F_{2g} mode of vibration where the atoms are loosely bound that can allow ion penetration.

Evidence for the improvement in the electrochemical performance of the Ni, Cr-doped sample is as follows: i) reduction in crystallite/grain size (as seen in XRD/FESEM analysis), ii) fast conduction path (decrease in charge-transfer resistance as seen in EIS spectra) which encourages the movement of ionic species thereby bringing a decrease in the internal resistance of the Ni, Cr-doped samples. Hence, in conclusion, Ni, Cr doped $ZnCo_2O_4$ performs better than the other two though it has a weaker point on diffusion.

9.7. Summary

Ni and Cr doped $ZnCo_2O_4$ have been prepared by sol-gel method and it exhibits spinel cubic phase with $Fd\bar{3}m$ space group. Rietveld refinement is made to arrive at the positional co-ordinates of zinc that have been changed due to the addition of Ni and Cr dopants from the pristine material. Furthermore, crystallite size decrement has been observed on doping also correlated with FESEM Micrographs.

Table 33 - Comparison of performance of the prepared undoped and doped $ZnCo_2O_4$

Performance	$ZnCo_2O_4$	Fe, Cr: $ZnCo_2O_4$	Ni, Cr: $ZnCo_2O_4$
Crystallite size (nm)	30.45	27.63	22.46
Specific capacitance (Fg^{-1})	266	320	575
Charge transfer resistance (Ω)	3.925	0.883	1.994
Cyclic stability (%)	82.2	94	90

The lattice loosening effect is observed with the peak merger of 649 cm^{-1} and 610 cm^{-1} which could be correlated to the diffusion of the ion on cycling. The electrochemical performance of the Ni and Cr doped $ZnCo_2O_4$ has been analysed with 1M KOH aqueous electrolyte solution, and it shows the specific capacitance value of 575 Fg^{-1} at the current density of 1 Ag^{-1} and capacitance retention of **90 % over 2000 cycles** and is higher than the pristine sample and Fe, Cr doped $ZnCo_2O_4$ with a capacitance retention of 94% over 2000 cycle. Table 33 gives the comparative performance of $ZnCo_2O_4$, Fe,Cr:$ZnCo_2O_4$, Ni,Cr:$ZnCo_2O_4$. In conclusion, the dopants such as Ni and Cr enhance the electrochemical performance of the pristine sample.